https://doi.org/10.5194/egusphere-2025-3479
Preprint. Discussion started: 25 July 2025

Culturing experiments reveal mechanisms of daily trace element incorporation into *Tridacna* shells

Authors: Iris Arndt[1,2], Jonathan Erez[3], David Evans[4], Tobias Erhardt[1,2], Adam Levi[3], Wolfgang Müller[1,2]

[1]Institute of Geosciences, Goethe University Frankfurt, Frankfurt am Main, 60316, Germany
[2]Frankfurt Isotope and Element Research Center (FIERCE), Goethe University Frankfurt, Frankfurt am Main, 60316, Germany
[3] Fredy & Nadine Herrmann Institute of Earth Sciences, Hebrew University of Jerusalem, Jerusalem, 9190401, Israel
[4]School of Ocean and Earth Science, University of Southampton, Southampton, SO171BJ, United Kingdom

Correspondence to: Iris Arndt (arndt@em.uni-frankfurt.de)

Abstract

Giant clams such as *Tridacna sp.* are exceptionally well suited for studying past environmental changes on various timescales, from daily to multidecadal. The visible growth bands in their shells, which can be yearly, seasonal or even daily, are accompanied by changes in the elemental composition of the shell and provide insights into their growth and environmental history. The daily elemental cycles, particularly in Mg/Ca and Sr/Ca, can be used to determine age and growth rates. However, the mechanisms creating the visible day and night banding and the associated elemental cycles, remain unclear. To better understand the mechanisms of El/Ca incorporation into the *Tridacna* shell during day and night growth, we performed controlled growth experiments using ^{135}Ba-labelled seawater. It was alternatingly applied in 12-hour intervals in order to individually and unequivocally mark day and night growth segments in *Tridacna*. These experiments show that *Tridacna* calcification rates are nearly five times higher during the day than at night. The bivalve's extrapallial fluid (EPF) reacts to changes in seawater chemistry within tens of minutes, both during day and night, with full compositional replenishment achieved after approximately one day. During daytime, El/Ca (for El = B, Mg, Sr, Ba) decrease, while Na/Ca increases. The opposite behaviour occurs at night. The night peak in El/Ca occurs in the earliest morning, shortly before the change between spiked and non-spiked water at 7:30. Daily El/Ca cycles are likely caused by variations in active Ca^{2+} and HCO_3^- transport into the EPF, influenced by light availability, circadian rhythms and/or energy availability (from both photosymbionts and filter feeding), rather than a closed-system Rayleigh fractionation process driven by contrasting El-distribution coefficients. We propose that active Ca^{2+} and HCO_3^- pumping into the EPF might also drive diurnal changes of growth rate, shell structure and possibly organic content.

1 Introduction

Giant clams serve as archives recording palaeoenvironmental changes in (sub)tropical reefs since their emergence in the middle Eocene, with *Tridacna* emerging in the early Miocene (Harzhauser et al., 2008). Their large, dense aragonitic shells are less prone to diagenetic recrystallisation compared to other reef organisms such as corals (Griffiths et al., 2013; Veeh and Chappell, 1970; Welsh et al., 2011). Additionally, *Tridacna* clams live for several decades (Arndt et al., 2025; Rosewater, 1965; Watanabe et al., 2004) and grow quickly, at rates ranging from millimetres to centimetres per year (Arndt et al., 2023; Bonham, 1965; Elliot et al., 2009; Fousiya et al., 2024; Fursman et al., 2025; Ma et al., 2020; Mills et al., 2023; Rosewater, 1965; Warter et al., 2018). This combination

https://doi.org/10.5194/egusphere-2025-3479
Preprint. Discussion started: 25 July 2025

of excellent preservability and quick growth makes them valuable for reconstructing past environmental changes on timescales from daily to multiannual (de Winter et al., 2023; Warter et al., 2015; Warter and Müller, 2017; Yan et al., 2021, 2020; Zhao et al., 2021), even for pre-Pleistocene 'deep time' periods. Decade-long, sub-daily-resolved records can be used to examine phenomena such as (palaeo-)ENSO, seasonal aspects of palaeoclimate as well as short-term extreme weather events (Arndt et al., 2025).

Tridacna are mixotrophic clams that can obtain nutrition via filter feeding and photosynthesis from the photosymbionts hosted in the soft tissue (Jantzen et al., 2008; Klumpp et al., 1992; Kunzmann, 2008). However, phototrophy is thought to be the main source of energy for the host (Klumpp and Griffiths, 1994). The balance between phototrophy and heterotrophy might be adapted depending on species (Jantzen et al., 2008) and turbidity of the habitat (Mills et al., 2023). Overall, light availability has a positive impact on calcification (Rossbach et al., 2019; Sano et al., 2012; Warter et al., 2018).

The shells of *Tridacna* contain visible patterns that provide insights into their growth and environmental history. Growth bands within the shell can represent different time intervals. Banding patterns on the millimetre to centimetre scale are visible to the naked eye and can be yearly growth bands (Ayling et al., 2015; Pätzold et al., 1991; Warter et al., 2015; Welsh et al., 2011) or seasonal growth bands, such as two bands per year (Arndt et al., 2025; Ma et al., 2020). Bands on the micrometre scale, visible under a microscope, show daily growth (Aharon and Chappell, 1986; Arndt et al., 2023; Hori et al., 2015; Pätzold et al., 1991; Warter et al., 2018; Watanabe and Oba, 1999; Yan, 2020). Banding patterns within the shell (both seasonal and daily) are linked to changes in the shell's microstructure (Brosset et al., 2025; Mills et al., 2024, 2023).

By counting the visible daily growth bands, the age and growth rates of giant clams can be determined (Duprey et al., 2015; Gannon et al., 2017; Sano et al., 2012; Zhao et al., 2023). *Tridacna* shells also exhibit daily compositional cycles, most prominently in Mg/Ca and Sr/Ca (Brosset et al., 2025; Hori et al., 2015; Sano et al., 2012; Warter et al., 2018; Warter and Müller, 2017; Yan, 2020). These elemental cycles can be detected even if daily bands are poorly visible, such as in fossil giant clams (Arndt et al., 2023). Therefore, elemental ratios can be used to help quantifying growth rates and determining the age, e.g. using the Daydacna Python script (Arndt et al., 2023; Arndt and Coenen, 2023). However, the causes for the visible day and night banding as well as the related cycles in El/Ca ratios remains unclear.

Between areas grown at day and night, differences in growth rate (Sano et al., 2012; Warter et al., 2018), shell structure (Agbaje et al., 2017; Brosset et al., 2025; Mills et al., 2024) and organic content (Liu et al., 2022) have been observed. The varying incorporation of elements into the shell between day and night might be linked to these observations and caused by associated physiological, environmental or chemical factors. There is a lack of studies that unequivocally discern El/Ca changes between day and night growth in *Tridacna* under controlled experimental conditions. To the best of our knowledge, the study by Warter et al. (2018) is the only one that demonstrated an increase in Sr/Ca and Mg/Ca during nighttime calcification in *Tridacna*, using isotopically-labelled seawater during an unintended nighttime culturing interruption. However, the study could not rule out potential stress-related factors that might have overprinted the results.

In this study, we expand on the previous work of Warter et al. (2018) and present the results of a specifically designed culturing experiment with *Tridacna* where day- and night-growth periods were individually and alternatingly marked using the isotopic tracer ^{135}Ba. Via spatially/time-resolved elemental analysis by LA-ICPMS at an unprecedented <2 µm resolution, the respective identification of day and nighttime trace elemental signatures of the shell was possible. ^{135}Ba and ^{87}Sr isotopic tracers have previously been used to identify specific growth

https://doi.org/10.5194/egusphere-2025-3479
Preprint. Discussion started: 25 July 2025

domains in foraminifera (Evans et al., 2016; Fehrenbacher et al., 2017; Hauzer et al., 2021, 2018; Levi et al., 2019) and giant clams (Warter et al., 2018). With the tracer experiment we gain unprecedented insights into changes in growth rate, elemental uptake from the surrounding seawater and element incorporation into the shell between day and nighttime.

2 Material and Methods

2.1 Culturing

Eight juvenile giant clams with lengths of 3 to 4 cm were purchased from an aquarium supplier and transported to the Hebrew University of Jerusalem, where all culturing experiments took place. Prior to the actual onset of the controlled day-night culturing experiments (see below), the clams' calcification performance was monitored over 15 days and conditions were optimised accordingly by adjusting water temperature, alkalinity, light availability and feeding.

The seawater used for the culturing of the clams was retrieved from the Gulf of Eilat. Its salinity was lowered to 37 psu by mixing 10 l of Eilat sea water (ESW), characterized by 40.7 psu, with 1 l of distilled water for each of the four 11 l seawater reservoirs, kept in separate plastic containers. Two of the 11 l reservoirs were spiked with 0.55 ml of dissolved $^{135}BaCO_3$ (240 $^{135}BaCO_3$ µg/ml; 93.5% enriched; Oak Ridge National Laboratory, USA) to create the 'spiked' seawater in which the naturally minor Ba-isotope ^{135}Ba (6.59% natural abundance) is more than tenfold enriched. Based on a [Ba] value of ESW of 9.9 ng/g (Evans et al., 2015), this yields a $^{135}Ba/^{138}Ba$ of approximately 1.24 in the 11 l of spiked, modified ESW. No accurate knowledge of this ratio is required other than being over tenfold higher than the natural $^{135}Ba/^{138}Ba$ of 0.092, as it solely serves to distinguish unequivocally between the respective growth increments of the cultured clams. Assuming a 10% range of [Ba] in ESW, the associated $^{135}Ba/^{138}Ba$ range of spiked, modified ESW is ~1.13 - 1.35, with Ba mass bias contributing another ~1.5% uncertainty only on this isotopic ratio, which is negligible in view of the ESW [Ba] uncertainty. Two further 11 l plastic containers with normal, non-spiked seawater were used. Night and day water was separated, hence the requirement for four different seawater reservoirs, namely 'night ^{135}Ba-spiked water', 'night non-spiked water', 'day non-spiked water' and 'day ^{135}Ba-spiked water'.

Initially, after purchase, all clams grew in natural ESW in a large aquarium but were then transferred to specific culturing jars. All clams underwent a 78-hour 'spiking' procedure. This included growing in the culturing jars with modified ESW enriched with ^{135}Ba isotope tracer for 42-hours under optimized growth conditions, i.e. minimal stress, and transferring them back to an ESW aquarium to grow in non-spiked water for 36 hours. The optimized conditions included initial alkalinity above 2 meq/kg, a temperature of 28 °C and coral food being added to the water.

All eight clams were cultured in pairs in four jars for a duration of 72 hours. The clams sample IDs include the jar number, the number of the clam within the jar and whether it is day (DAS) or night (NIS) spike treatment (Tab. 2). For example, sample "1.1 NIS" refers to the first jar, first clam that received ^{135}Ba-spiked water at night. Please note that the laboratory sample ID is based on markings drawn on the shells for differentiation during culturing, and it differs from the sample ID used in the paper (see Table S1). The jars with a water capacity of 630 ml were sealed airtight and placed in a temperature bath. Water was pumped through the jars with a rate of 210 ml/h, resulting in a 3 h residence time. All jars were kept under the same conditions regarding light, temperature and salinity. The clams were exposed to light with an intensity of 400 µE (measured on top of the jars) for 12 h, from

https://doi.org/10.5194/egusphere-2025-3479
Preprint. Discussion started: 25 July 2025

7:30 to 19:30. The temperature was kept at 28 °C. The four jars were exposed to an alternating sequence of ^{135}Ba-
120 spiked and non-spiked water (Fig. 1). Jars 1 and 2 were exposed with seawater spiked with ^{135}Ba during the night (19:30 to 7:30), while non spiked seawater was present in jars 3 and 4 at night. During the day (7:30 to 19:30) jars 1 and 2 were filled with non-spiked seawater, while jars 3 and 4 were exposed to seawater spiked with ^{135}Ba.

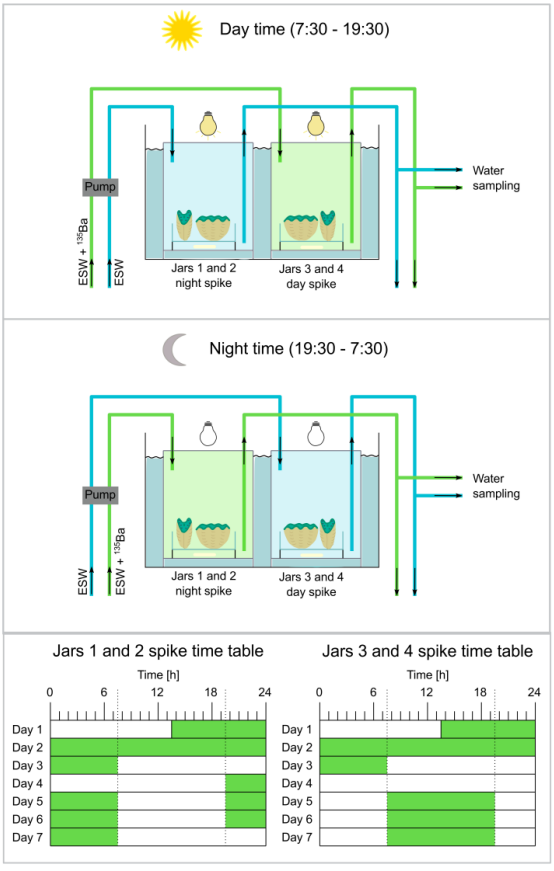

Figure 1: Experimental setup of the culturing tanks: A: Setup during daytime, jars number 1 and 2 (represented by
125 **one jar in the sketch) contain Eilat Sea Water (ESW) while ESW spiked with the ^{135}Ba tracer is introduced into jars number 3 and 4 from 7:30 to 19:30. During this time, the lights over the culturing jars are on. B: During nighttime (19:30 to 7:30) the source is reversed: ESW spiked with the ^{135}Ba tracer is introduced into jars number 3 and 4, while jars number 1 and 2 receive non-spiked ESW and the lights remain off. A transition period where water is pumped in and out of the jars takes place in the mornings and evenings from ~7:00 to 7:30 and 19:00 to 19:30, respectively. Each**
130 **jar contains two clams sitting on a petri dish each. The water within the jars is stirred with a magnetic stir bar. C: Timing of the alternating seawater exposure between ^{135}Ba-spiked and non-spiked water (the green shaded blocks indicate ^{135}Ba-enriched seawater) for all four jars: After the initial spiking period of 72 hours, 3 and 4 received spiked water during the day from 7:30 to 19:30 - as indicated by the dashed line. Jars 1 and 2 received the opposite spiked seawater treatment.**

135 The initial reservoir water was recycled, by mixing the outflow from the jars with the remaining respective reservoir water, and aerated for 15 min. The reservoir waters were sampled every morning and evening, before the new water source was connected. Final outflow water samples were taken directly from the jar outflow before the lights turned on in the morning and off in the evening.

https://doi.org/10.5194/egusphere-2025-3479
Preprint. Discussion started: 25 July 2025

Oxygen, pH and alkalinity measurements were performed every 12 hours on both the initial and final water samples. Resulting differences, namely Δoxygen, ΔpH and Δalkalinity, for each jar are displayed in table 2. Oxygen was monitored via an YSI ProODO meter, pH was measured using a WTW pH 340i ph-meter and alkalinity measurements were undertaken using a Metrohm 716 DMS titrino device. The alkalinity difference between the beginning and end value of the experiments was used to calculate the $CaCO_3$ uptake and the resulting percentage of growth per day and clam (see Table 2).

After the clams were sacrificed, the shells were separated from the soft tissue and brushed clean using tap water. The clean shells were embedded in resin and cut along the maximum growth axis. Thin sections with a thickness of 50 µm were prepared and polished using a 3 µm diamond suspension.

2.2 Spatially-resolved elemental analysis by LA-ICPMS

Laser-ablation inductively-coupled-plasma mass spectrometry (LA-ICPMS) was performed on thin sections (50 µm thick) using a novel custom-built dual-wavelength (157 & 193 nm) LA–ICP–MS/MS system, operated at 193 nm, coupled to an inductively coupled plasma tandem mass spectrometer, operated in single-quadrupole mode (Erhardt et al., in revision, JAAS). More specifically, this comprises a modified RESOlution-SE LA-system (Applied Spectra Inc., formerly Resonetics LLC), featuring a Coherent ExciStar 500 excimer laser (instead of an Atlex ATL laser) and a Laurin Technic S-155 two-volume LA cell (Müller et al., 2009) that is linked to an Agilent 8900 ICP-MS/MS. Ablation took place in an He atmosphere (0.35 l/min) to which Ar (1.00 l/min) was added, besides N_2 (3.5 ml/min) to enhance sensitivity and plasma stability (see Table S2). LA-ICPMS instrument tuning used a 50 µm round spot, with 10 Hz and 3 J/cm^2 on NIST SRM612 to achieve tuning parameters of 0.07% oxide rate (ThO^+/Th^+), 0.5% doubly-charge rate (22/44), 0.18 $^{38}Ar/^{80}Ar$ and 99% $^{232}Th/^{238}U$ ratio with an ^{238}U-signal of around 1 Mcps. The analyses were broadly based on the methodology in Warter et al. (2018) by performing laser ablation in slow continuous profiling mode with a rotatable slit and LA tracks that were set in direction of growth starting at the final growth segments of the outermost shell (Fig. 2). To maximize spatial resolution while maintaining suitable instrument sensitivity that is crucial in view of low Ba concentrations of around 2 µg/g, we used a rotating rectangular mask that resulted in a 1.25 × 50 µm laser spot on the sample. The ablation area is equivalent to a 9 µm round laser spot and thus provides more than sevenfold improved spatial resolution, which is essential to resolve the daily growth segments ranging between ~5 to 20 µm. The rotatable slit was aligned to be parallel to the daily banding throughout the measurements (Fig. 2). Differing from Warter et al. (2018), the laser and ICPMS settings were optimized to match the 800 ms washout time of the sample introduction system (full width at 1% maximum of the single pulse response). To do so, the overall ICPMS sweep time was set to 206 ms for the following monitored isotopes (and dwell times): m/z ^{11}B (37 ms), ^{23}Na (16 ms), ^{24}Mg (18 ms), ^{43}Ca (16 ms), ^{88}Sr (16 ms), ^{135}Ba (47 ms) and ^{138}Ba (42 ms). In turn, the laser beam was scanned at 1.517 µm/s to yield four sweeps per laser beam width, with the laser trigged five times during every sweep using a QuadLock device (Norris Scientifc (Norris et al., 2021)), resulting in a repetition rate of 24.27 Hz. The QuadLock aligns the laser firing rate to the ICPMS, eliminating any aliasing artifacts in the data (Norris et al., 2021). The on sample fluence was set to ~4.5 J/cm^2. Each ablation track was pre-cleaned with 100 Hz repetition rate with a spot overlap of 90%, i.e. ten shots deep.

https://doi.org/10.5194/egusphere-2025-3479
Preprint. Discussion started: 25 July 2025

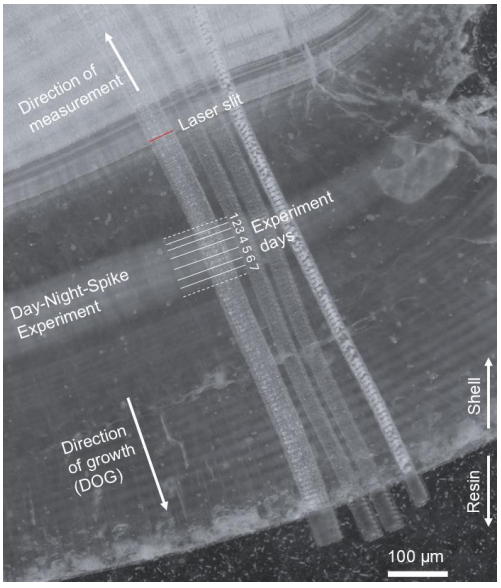

Figure 2: Microscope image of the thin section of sample 3.1 DAS with laser-ablation paths, of which the leftmost reflects the data presented in this study. The brighter shaded domain that represents the day-night bands is indicated, including experiment days; following the experiment reported herein, the shells continued growing in a different experimental setup whose results are beyond the scope of this study, and which will be reported elsewhere. The rotatable 1.25 x 50 µm laser slit, indicated by the red bar, is set parallel to the daily bands, with the laser-ablation path progressing parallel (but opposite to) the direction of growth.

The measurements were quantified following Longerich et al. (1996) using NIST SRM612 as external standard, with the reference values from Jochum et al. (2011), except for Mg for which the updated value of 62.4 µg/g from Evans and Müller (2018) was used. ^{43}Ca was used as internal standard.

Processing and visualization of LA-ICPMS data were performed utilizing the Iolite 4 software (Paton et al., 2011) and Python, with the support of libraries such as NumPy (Harris et al., 2020), Pandas (Reback et al., 2022) and Matplotlib (Caswell et al., 2022).

To evaluate data quality, i.e. accuracy and precision, measurements were taken of the carbonate standard MACS-3 nanopellet and the MPI-DING glass standard K2L-G. For MACS-3, boron reference values are taken from LA-ICPMS data (Jochum et al., 2012), while the Na, Mg, Sr, Ba reference values are solution based USGS-data from Stephen Wilson (pers. comm, 2010). For KL2-G we use the preferred values from GeoReM database 658 (Jochum et al., 2006). These standards were measured and processed in the same way as the samples. Accuracies range from -2.2 to -13.0% for MACS-3NP and -7.4 to 15.5% for KL2-G, while precision ranged between 1.5 and 10.8% 2 RSD for MACS-3NP and 1.8 and 22.2% 2 RSD for KL2-G (see Table 1).

https://doi.org/10.5194/egusphere-2025-3479
Preprint. Discussion started: 25 July 2025

Table 1: Assessment of analytical accuracy and precision based on repeated measurements of the carbonate standard MACS-3 and the glass standard KL2-G. Reported values include measured means and associated ±2 SD, compared to reference values from literature (Jochum et al., 2012 (for MACS-3 B); Jochum et al., 2006 (for KL2-G) ; Stephen Wilson, pers. comm., 2010 (for MACS-3 Na, Mg, Sr, Ba)). Accuracy is expressed as the deviation from the reference value, and precision as the reproducibility (±2 % RSD) of the measurements.

MACS-3	Measured mean [µg/g]	± 2 SD [µg/g]	Reference value [µg/g]	± 2 SD [µg/g]	Accuracy [%]	Precision [% 2 RSD]
B	8.63	0.47	8.90		-3.0	10.8
Na	5133	240	5900	800	-13.0	9.2
Mg	1717	45	1756	272	-2.2	5.2
Sr	6396	140	6760	700	-5.4	4.5
Ba	56.3	0.6	58.7	4.0	-4.1	2.3
KL2-G	**Measured mean [µg/g]**	**± 2 SD [µg/g]**	**Reference value [µg/g]**	**± 2 SD [µg/g]**	**Accuracy [%]**	**Precision [% 2 RSD]**
B	3.15	0.35	2.73	0.28	15.5	22.2
Na	16136	820	17434	593	-7.4	10.2
Mg	42628	2000	44263	543	-3.7	9.4
Sr	352	3	356	8	-1.0	1.8
Ba	121.1	1.8	123.0	5.0	-1.5	3.0

3 Results

3.1 Water parameters

A clear pattern between night and daytime calcification is seen in the difference in seawater carbonate chemistry and dissolved [O_2] measured in the evening and morning. During daytime, pH increases by ~0.14 units while oxygen concentrations rise by ~1 mg/l. At the same time, water alkalinity is reduced by 80 µmol/kg on average, equivalent to a calcification rate of 0.09 wt% growth (weight increase) per clam for this 12 h interval. The shell weight was estimated as 60% of the measured weight of the clam with soft tissue and the resulting average shell weight of 5 g was used to calculate the calcification rate. In contrast, during the night, pH decreases by 0.17 and oxygen concentrations are ~1.35 mg/l lower than in the morning, compared to the previous evening. The average water alkalinity reduction is only 16 µmol/kg, resulting in an average calcification rate of 0.02 wt% per clam per 12 h. While the clams calcify both during day and night, the daytime calcification rates are almost fivefold (4.5 to 5 times) higher.

https://doi.org/10.5194/egusphere-2025-3479
Preprint. Discussion started: 25 July 2025

Table 2: Changes in water chemistry and calcification rates of the clams that were alternatingly exposed to ^{135}Ba-spiked and non-spiked seawater for 12 h each during daytime and nighttime. The table indicates which clams were cultured in each jar, the spike condition (presence or absence of ^{135}Ba), and the measured differences in pH, oxygen, and alkalinity over 12-hour intervals. Calcification rates were calculated from alkalinity changes and are expressed as percentage of growth per clam per 12 hours. The average calcification of all eight clams is provided for every day and night interval.

	Jar	Clams	Spike	Δ pH	Δ oxygen	Δ Alkalinity [µMol]	Calcification [%/clam and 12h]	Average calcification [%/clam and 12h]
Night 4	J1	1.1 NIS, 1.2 NIS	^{135}Ba	-0.189	-1.82	11	0.013	0.02
	J2	2.1 NIS, 2.2 NIS	^{135}Ba	-0.188	-1.84	13	0.017	
	J3	3.1 DAS, 3.2 DAS		-0.208	-0.73	20	0.023	
	J4	4.1 DAS, 4.2 DAS		-0.2055	-1.37	16	0.019	
Day 5	J1	1.1 NIS, 1.2 NIS		0.1325	0.83	89	0.103	0.1
	J2	2.1 NIS, 2.2 NIS		0.1395	1.18	86	0.106	
	J3	3.1 DAS, 3.2 DAS	^{135}Ba	0.1405	1.03	80	0.092	
	J4	4.1 DAS, 4.2 DAS	^{135}Ba	0.1785	1.07	85	0.101	
Night 5	J1	1.1 NIS, 1.2 NIS	^{135}Ba	-0.1865	-1.67	24	0.028	0.02
	J2	2.1 NIS, 2.2 NIS	^{135}Ba	-0.2035	-1.86	21	0.026	
	J3	3.1 DAS, 3.2 DAS		-0.2055	-1.38	16	0.019	
	J4	4.1 DAS, 4.2 DAS		-0.1755	-1.26	10	0.012	
Day 6	J1	1.1 NIS, 1.2 NIS		0.1885	0.23	85	0.098	0.09
	J2	2.1 NIS, 2.2 NIS		0.1685	0.31	70	0.087	
	J3	3.1 DAS, 3.2 DAS	^{135}Ba	0.1455	0.95	74	0.085	
	J4	4.1 DAS, 4.2 DAS	^{135}Ba	0.1465	1.08	72	0.085	
Night 6	J1	1.1 NIS, 1.2 NIS	^{135}Ba	-0.1335	-0.91	19	0.022	0.02
	J2	2.1 NIS, 2.2 NIS	^{135}Ba	-0.1105	-0.82	13	0.016	
	J3	3.1 DAS, 3.2 DAS		-0.1235	-1.31	21	0.024	
	J4	4.1 DAS, 4.2 DAS		-0.1215	-1.18	12	0.015	
Day 7	J1	1.1 NIS, 1.2 NIS		0.118	0.95	95	0.11	0.09
	J2	2.1 NIS, 2.2 NIS		0.121	1.12	64	0.08	
	J3	3.1 DAS, 3.2 DAS	^{135}Ba	0.127	1.31	79	0.091	
	J4	4.1 DAS, 4.2 DAS	^{135}Ba	0.0945	0.89	79	0.094	

3.2 Spatially-resolved compositional data (LA-ICPMS)

The elemental ratio data from the day-night spiking experiment can be found in Table S3 and are displayed in Figure 3. Overall, the B/Ca values span from 0.04 mmol/mol to 0.34 mmol/mol, with an average of 0.13 mmol/mol. Na/Ca values range between 17.2 to 29.8 mmol/mol, with an average of 24.0 mmol/mol. Mg/Ca values vary nearly tenfold between 0.25 and 2.21 mmol/mol, with an average of 0.77 mmol/mol. The average Sr/Ca value is 1.57 mmol/mol, with a minimum of 0.82 and maximum at 2.4 mmol/mol. Ba/Ca values vary from 0.21 to 2.09 µmol/mol, with an average of 0.77 µmol/mol. (Fig. 3).

https://doi.org/10.5194/egusphere-2025-3479
Preprint. Discussion started: 25 July 2025

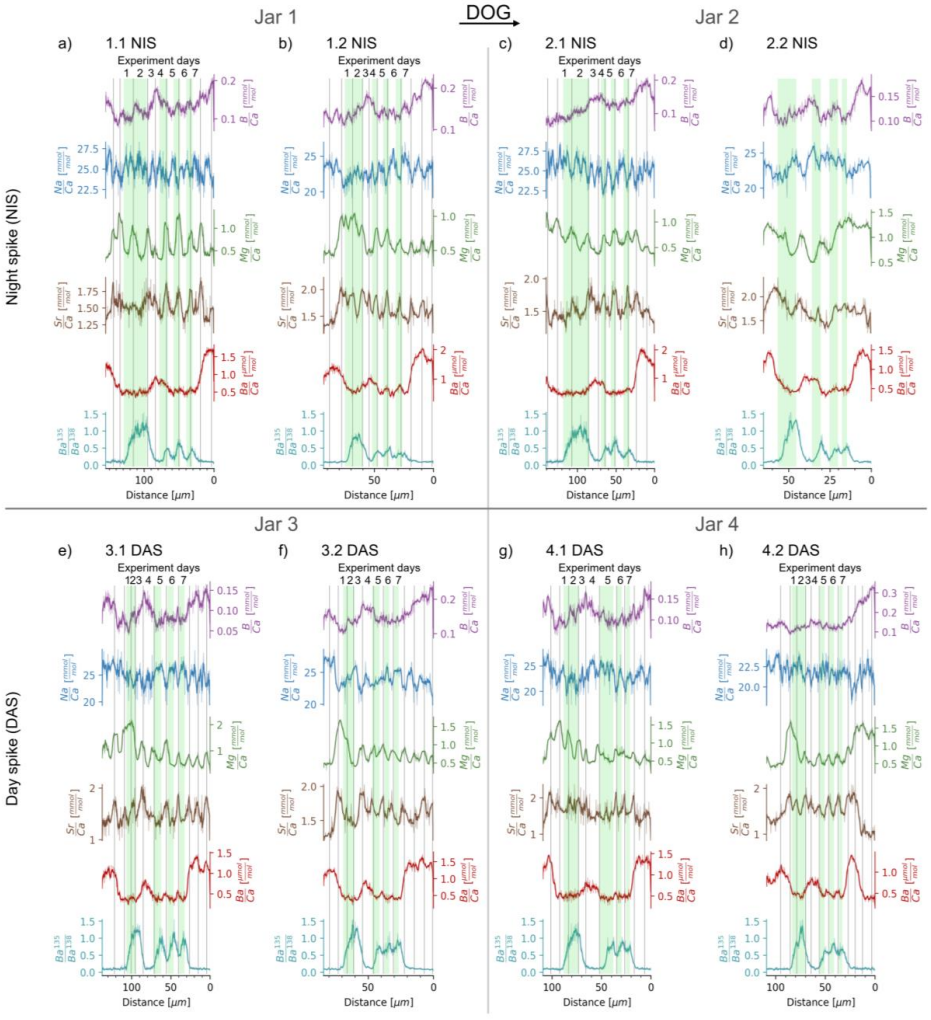

Figure 3: Spatially-resolved El/Ca (B, Na, Mg, Sr, Ba) and $^{135}Ba/^{138}Ba$ isotopic ratios for all cultured clams. The latter varies between the natural ratio of 0,092 and approaches that of the spiked water of ~1.24. Datasets a-d) represent the shells grown with ^{135}Ba-spiked water during the night at experiment days 4 to 6 ('NIS'), with two jars and two clams per jar. Datasets e-h) represent the shells that were given the ^{135}Ba-spiked water during the day from days 5 to 7 ('DAS'), also with two jars and two clams per jar. Areas grown during exposure to ^{135}Ba-spiked water are indicated by green bars. $^{135}Ba/^{138}Ba$ intake during the 12 h interval is higher for day-spiked clams than night-spiked clams. Daily cycles are visible in Mg/Ca and Sr/Ca for 7 out of 8 clams. Clam 2.2 NIS grew only about half compared to its 'partner clam' 2.1 NIS and does not display daily cycles. For the other 7 shells, vertical lines indicate Mg/Ca maxima, and if uncertain, Sr/Ca maxima, which thus delineate the daily growth increments. Note that the x-y axis scaling is not uniform between the clams but optimized for best data visibility, with the exception of $^{135}Ba/^{138}Ba$.

The initial introduction of the clams to ^{135}Ba-spiked water of 42 h on experiment day 1 and 2 shows that most shells do reach a $^{135}Ba/^{138}Ba$ plateau close to the calculated $^{135}Ba/^{138}Ba$ ratio of the water of ~1.24 after 24 h. However, shells NIS 1.2 and NIS 2.1 only reach $^{135}Ba/^{138}Ba$ plateau values of ~0.8 and 1.0, while DAS 3.2 and DAS 4.2 reach 1.3 and 1.4, respectively. The latter might indicate that the $^{135}Ba/^{138}Ba$ ratio of 1.24, calculated for the spiked water, was slightly underestimated by overestimating the initial ESW [Ba]. At experiment day 7, after the last exposure to the spiked water, the $^{135}Ba/^{138}Ba$ ratio returns to a ratio of ~0.1, approaching the natural ratio

https://doi.org/10.5194/egusphere-2025-3479
Preprint. Discussion started: 25 July 2025

of 0.092, within 24 h in the night-spiked and within 12 h in the day-spiked clam shells. The data from experiment days 4 to 7 show that ^{135}Ba is incorporated into the shells of clams subjected to the tracer both during the day (7:30 to 19:30) as well as during the night (19:30 to 7:30). The $^{135}Ba/^{138}Ba$ ratio delineates the relative growth between day and night, with daytime ^{135}Ba uptake being on average 1.7 times higher than nighttime ^{135}Ba uptake. This is because of the contrasting cyclical $^{135}Ba/^{138}Ba$ ratio variations of 0.2 to 0.7 and 0.4 to 1.1 for night and day-spiked clams, respectively.

In most clams Mg/Ca and Sr/Ca show a regular cyclicity that can be clearly identified as daily, based on the timing of the isotopic tracer introduction. Unequivocally, both show the highest values during nighttime (Fig. 4a). Daily cyclicity is less clear in Na/Ca, for which the nighttime growth seems to be characterised by domains with low Na/Ca, while higher Na/Ca is reached during the day. In B/Ca and Ba/Ca daily cycles are less clear and the ratios vary strongly between parts grown in the aquarium and the culturing jars. The shells were growing in a large ESW aquarium with other clams and corals before experiment day 1 and after experiment day 7; they resided in a smaller separate aquarium with ESW at experiment days 3 to 4 and in the culturing jars with modified (reduced salinity) ESW during experiments days 1 to 2 and 5 to 7. The observed changes in B/Ca and Ba/Ca (Fig. 3) are likely caused by slightly different seawater compositions in the different growth environments.

We observe that Mg/Ca and Sr/Ca and less clearly B/Ca and Ba/Ca are in phase with $^{135}Ba/^{138}Ba$ for night-spiked shells (e.g. in NIS 1.1, Fig. 4a). In contrast, day-spiked shells display an anti-phased relationship (e.g. in DAS 3.1, Fig. 4b). Therefore, a ^{135}Ba increase at night is seen in the shell, approximately coinciding with the minimum to maximum of both Mg/Ca and Sr/Ca cycles. In contrast, the increase in ^{135}Ba during the day coincides with (or shortly postdates) the shift from the Mg/Ca (or Sr/Ca) maximum to respective minimum (or shortly thereafter in each case).

https://doi.org/10.5194/egusphere-2025-3479
Preprint. Discussion started: 25 July 2025

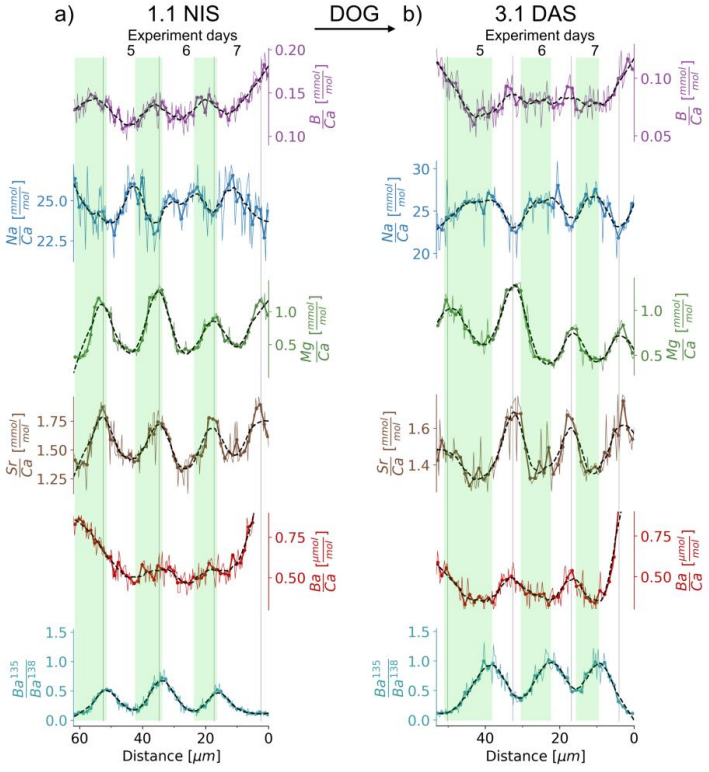

Figure 4: Expanded view of El/Ca and $^{135}Ba/^{138}Ba$ ratios for the sections of the shell grown during the day-night-spiking of two representative examples, namely 1.1 NIS and 3.1 DAS. A 4-point running mean is plotted in addition to the original data. Each 4-point-mean data point is indicated by a circle, resulting in one circle every 1.25 µm which is the same as the width of the laser beam. The red dashed line represents a quadratic polynomial fit to the 4-point-mean signal using a Savitzky-Golay filter (Savitzky and Golay, 1964), which smooths the data while preserving important features of the signal.

4 Discussion

4.1 Reproducibility

In the experimental setup all eight clams grew in the same environmental conditions such as temperature, light and food availability, and only the timing of ^{135}Ba-spiked water introduction was systematically varied. Four clams in two jars received a ^{135}Ba-spike at night and daytime, respectively. The initial water reservoir, later divided into spiked and non-spiked, was the same. Some patterns consistently emerge between the two sets of four replicates, such as the overall incorporation of the isotopic tracer, daily elemental cycles and changes between aquarium and culturing water (Fig. 3). On a more detailed level, there are clear differences between the individual clams regarding overall growth, growth pattern and element incorporation even between pairs kept within the same jar (see 1.1 vs 1.2 NIS, 2.1 vs 2.2 NIS, 3.1 vs. 3.2 DAS), presumably related to their individual physiology. During the seven days of experiment, the clams' shells grew between 55 to 115 µm in the direction of growth. Similarly, daily growth rates range from 6 to 21 µm/day and vary by up to 9 µm/day even within one clam (Fig. 3e).

https://doi.org/10.5194/egusphere-2025-3479
Preprint. Discussion started: 25 July 2025

4.2 Analytical resolvability

Given a sweep time of 0.206 s and a scan speed of 1.517 µm/s, the resulting sampling frequency is 0.313 µm. With a slit width of 1.25 µm this results in four sampling points per slit with. If we use the 4-point mean values, i.e. one data point per slit width, to get independent data points, we can safely detect cycles above 3 µm wavelength. As daily cycle wavelengths range from 6 to 20 µm, all compositional cycles should analytically be well resolved.

The full signal rise takes 0.2 s i.e. 0.3 µm in sampling direction and signal washout to 10% and 1% takes place in 0.5 s and 1.2 s (0.8 and 1.8 µm in sampling distance), respectively. Therefore, data points in 1.25 µm steps (~0.8 s measurement time) are not completely independent but can contain ~ 5% of the signal from the previous data point. As the resulting measured signal consist to 95% of the actual signal at that distance, we do not expect washout to lead to significant signal alteration.

Using a narrow but wide laser slit (1.25 x 50 µm) helps to obtain suitably high elemental signals for low [Ba] and [B] while maintaining very high spatial resolution (<2 µm). With a narrow, long slit optical alignment to daily banding is facilitated as misalignment is easy to see, however slight variations from the alignment might result in minor signal mixing between growth layers. In some shell areas the daily band structures are either slightly bent or not visible at all (Fig. 2). We aimed to position the laser slit as parallel as possible to the daily banding, avoiding bent structures. Quantitatively, if the slit is 2° misaligned, it would cover ~3 µm in direction of growth, while 5° result in almost 6 µm, so more than four times the laser slit width. We evaluated the microscope pictures of the laser ablation paths on the shells. As the day-night-experiment is well visible through a lighter shading in the shell (likely due to higher temperatures and faster growth rates compared to the aquarium; Fig. 2) an accurate alignment was possible. We deduce that we measured parallel to the daily banding with occasional offset between laser slit and growth banding direction of below 2°. Therefore, analytical signal smoothing could have occurred in some areas but would be constrained to areas of 3 µm or less, which is still half the minimum daily growth width.

Nevertheless, the dataset contains areas with unclear El/Ca signals on scales of tens of µm, e.g. in Mg/Ca days 1 to 2 of DAS 4.1, Sr/Ca days 1 to 2 of NIS 1.1 and in Mg/Ca throughout NIS 2.2 (Fig. 3). Interestingly, at the same distance, the cycles in the other respective ratios (Sr/Ca, Mg/Ca and $^{135}Ba/^{138}Ba$) are resolvable. This is an additional indicator to exclude analytical smoothing of the signal as the reason for these unclear cycles. We therefore deduce that the unclear cyclic patterns are not analytically caused but reflect the clams' individual growth performance and elemental uptake into the shell.

4.3 EPF reaction and replenishment time

The cyclic behaviour of the $^{135}Ba/^{138}Ba$ ratio within the shells, contrasts that of the rapid switch between the endmembers of spiked ($^{135}Ba/^{138}Ba$ = 1.24) and non-spiked ($^{135}Ba/^{138}Ba$ = 0.092) water (Fig. 5). In most shells, it takes about one day (i.e. ~5 to 20 µm of growth depending on the specimen) until the Ba isotopic ratio of the spiked water is reached. This smoothing is again unlikely to be caused by limited analytical resolvability because it is similar in all clams and above the worst case of analytically induced smoothing of 3 µm. We thus deduce that the $^{135}Ba/^{138}Ba$ ratio behaviour indeed reflects the uptake patterns of elements into the EPF.

During the day-night-spiking, i.e. experiment days 4 to 7, the uptake of the ^{135}Ba-isotopic tracer starts shortly after the Mg/Ca maximum (night spike) or minimum (day spike) is reached and $^{135}Ba/^{138}Ba$ continues to rise until the Mg/Ca minimum (night spike) or maximum (day spike). During the 12 h of culturing, the amount of ^{135}Ba-isotopic tracer continuously increases in the EPF such that the $^{135}Ba/^{138}Ba$ value of the shell continuously rises. Similarly, washout happens rapidly as indicated by a reduction of $^{135}Ba/^{138}Ba$ right after the Mg/Ca minimum (night spike)

https://doi.org/10.5194/egusphere-2025-3479
Preprint. Discussion started: 25 July 2025

or maximum (day spike) is reached. Taken together, we can unambiguously determine that the uptake of the spike occurs more quickly during daytime. Samples spiked during the day are broadly characterised by 1.7 times higher $^{135}Ba/^{138}Ba$ ratios which do not return to the baseline (i.e. natural) $^{135}Ba/^{138}Ba$ at night. This indicates that the residence time of Ba in the EPF is substantially shorter during the day than at night. Assuming barium and calcium behave similarly, this aligns with our alkalinity measurements described above which constrain a fivefold increase in calcification rate.

Despite a short EPF reaction time, indicated by rapid initial increase or decrease of the tracer within the shell, the time needed to reach the maximum $^{135}Ba/^{138}Ba$ value is approximately one day, as also indicated by the initial 42 h tracer exposure (Fig. 5). This further supports the idea of continuous exchange between seawater and EPF and, for these small specimens, indicates a barium (and calcium) residence time in the EPF of ~24 hours. Future work could test whether the residence time is longer for larger clams with a larger extrapallial volume, or whether the residence time is maintained as the result of a more efficient replenishment of the more voluminous EPF.

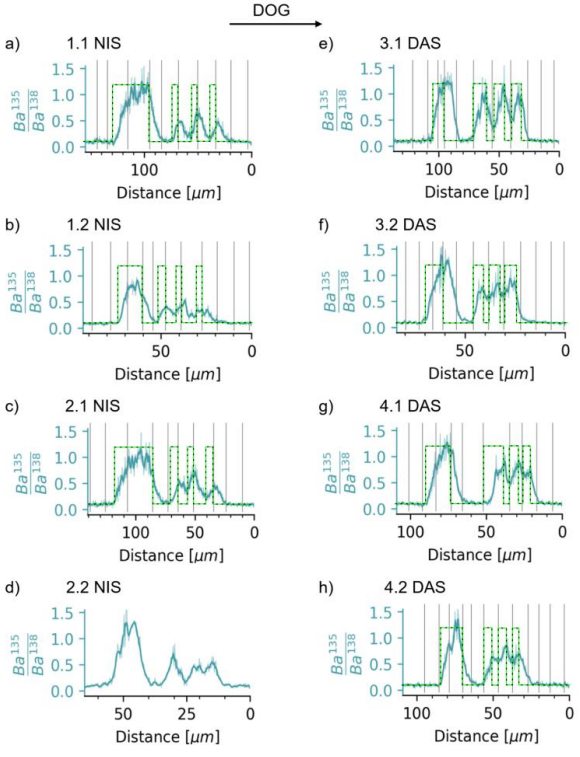

Figure 5: Measured $^{135}Ba/^{138}Ba$ ratios of all clams compared with the phases of ^{135}Ba-spiked water introduction, marked as a green-dashed rectangular function with the two endmembers being the natural $^{135}Ba/^{138}Ba$ ratio of 0.092 and the calculated $^{135}Ba/^{138}Ba$ of the spike water of 1.24. The shape of the measured $^{135}Ba/^{138}Ba$ ratio (blue) mostly reflects the uptake behaviour of Ba and other elements from the surrounding seawater into the EPF.

4.4 Causes for daily El/Ca cycles

In the following we discuss which of the possible environmental, biochemical and physiochemical factors have the clearest impact on daily El/Ca ratios. While these factors are inherently interconnected and often exhibit

https://doi.org/10.5194/egusphere-2025-3479
Preprint. Discussion started: 25 July 2025

complex interactions, they will be discussed separately to facilitate a clearer and more detailed understanding of their potential contributions.

4.4.1 Environmental factors

In natural environments linked parameter patterns can occur, e.g. temperature and light positively affect growth rate in *Tridacna* up to a stress limit (Killam et al., 2021; Schwartzmann et al., 2011; Van Wynsberge et al., 2017; Warter et al., 2018). Besides temperature and light, a further environmental factor that can impact daily elemental cycles is the availability of food that can be acquired through filter feeding. In reef environments dissolved oxygen concentrations, which broadly reflect net productivity and thus food availability, fluctuate diurnally. Concentrations are lowest at night, rising due to photosynthesis after sunrise, peaking in the afternoon, and then declining due to respiration and oxygen degassing (Silverman et al., 2007). However, given that *Tridacna* have photosymbionts and generally rely heavily on phototrophy, albeit with some species and environment-dependent variability (Jantzen et al., 2008; Klumpp and Griffiths, 1994; Mills et al., 2023), light may be a more important environmental driver of shell chemistry. It has been proposed that despite higher nutrient availability in the water at daytime, *Tridacna* rely more on photosynthesis for nutrition during the day and more on filter feeding during the night (Killam et al., 2023). Giant clams grown in culture experiments in which temperature and nutrient concentrations were not varied between day and night still show daily cycles (Warter et al., 2018; Figs. 3,4). We therefore deduce that temperature and nutrient availability are not the key driver of heterogeneity in shell chemistry in *Tridacna*.

As this is the case, light availability is a more likely explanation for the daily variability in shell growth and element incorporation, especially given that light enhanced calcification has been observed in *Tridacna* (e.g., Ip et al., 2015; Rossbach et al., 2019; Sano et al., 2012). Recent biochemical studies investigated elemental channelling through the mantle tissue within the context of the light dependent expression of channelling proteins relevant for shell formation. Multiple light enhanced calcium and bicarbonate transport mechanisms that could result in this phenomenon are active in shell formation, including voltage-gated calcium channels, Na^{+}/Ca^{2+} exchangers, plasma membrane Ca^{2+}-ATPase, and bicarbonate transporters (Boo et al., 2022, 2021; Cao-Pham et al., 2019; Chan et al., 2021; Chew et al., 2019; Ip et al., 2017, 2015).

4.4.2 Biochemical factors

Organic material present at the calcification site or involved in 'templating' the growing shell, might be important in driving shell chemistry. During daytime, calcification is faster and less templating organic matter might be incorporated into the mineral component of Tridacnid shells, while thinner bands, presumably grown at nighttime, are characterized by comparatively higher templating organic content (Liu et al., 2022). However, more dissolved organic matter might be incorporated during faster growth. In the case of inorganic calcite, the addition of certain organic molecules (peptides) has been shown to increase both growth rate and Mg-incorporation by reducing the dehydration enthalpy of Mg^{2+} to a greater degree than Ca^{2+}, resulting in increased Mg uptake (Stephenson et al., 2008). As organic material in *Tridacna* is present to a greater degree in the lower growth, nighttime bands with higher Mg/Ca, we assume that the availability of organic material is not a limiting factor in determining shell growth rate on a daily basis. Irrespective, the incorporation of organic material could conceivably be important in controlling shell chemistry (to a degree) given that the concentration of key elements typically considered to primarily substitute for Ca^{2+} in the mineral lattice may also be present in organics at relatively high concentration

https://doi.org/10.5194/egusphere-2025-3479
Preprint. Discussion started: 25 July 2025

For example, seasonal growth bands in *Artica islandica* and *Acesta excavata* are associated with increased organic contents and Mg^{2+} bound to the organic material, leading to increased Mg/Ca ratios during LA-ICPMS measurements (Schleinkofer et al., 2021; Schöne et al., 2010). It has also been suggested that seasonal Sr/Ca variability in *A. islandica* shells is controlled by the organic matrices at the calcification site (Shirai et al., 2014). However, given the absence of the (trace) elemental composition of Tridacnid organic material, we cannot assess the degree to which this could drive daily chemical banding.

Additionally, it has been shown that amorphous calcium carbonate (ACC) acts as a precursor phase in the biomineralisation of at least some bivalves (Addadi et al., 2006; Weiss et al., 2002). Organic material is incorporated into ACC, although the small amount of existing research has shown opposing impacts on Mg incorporation. Wang et al. (2009) found an increase in ACC Mg/Ca when organics are added, while Evans et al. (2020) found that adding amino acids reduced Mg/Ca. The latter explained the reduction in Mg/Ca with a preferential binding of Mg^{2+} with amino acids in solution and thus less Mg being incorporated (Evans at al. 2020). Irrespective, it is agreed that Mg^{2+} binds with amino acids to ligand-ion complexes to a differential degree to Ca^{2+}, such that this phenomenon has the potential to impact shell chemistry in organisms that utilise an amorphous precursor. Determining the direction in which this effect may act would require assessing the competing effects of co-incorporation of metals with organics into ACC and during crystallisation versus the impact that organics have on the Mg^{2+}/Ca^{2+} solution activity ratio (and therefore ACC and aragonite Mg/Ca), which is beyond the scope of this study. Studies on Tridacnid shell growth have shown that the shell ultrastructure varies between day and night growth (Agbaje et al., 2017; Brosset et al., 2025; Mills et al., 2024). These shell structures are associated with organic matrix components (Kobayashi and Samata, 2006) and have been interpreted to be caused by the variability in growth rate and possibly also organic content (Mills et al., 2024).

4.4.3 Physicochemical factors

A diurnal change in the physiological performance of the clams, regarding the replenishment of the EPF, indicates the possibility that elemental cycles are caused by non-uniform depletion of the EPF. This Rayleigh fractionation-type behaviour (Elderfield et al., 1996; Evans et al., 2018; Ram & Erez 2025) would potentially be visible if the rate of supply versus consumption of ions to the calcification site differed during the night compared to the day. In the case that Rayleigh distillation was a key control of shell trace element chemistry, we would expect elements with partition coefficients (K_d=El/$Ca_{aragonite}$ / El/Ca_{sw}) below 1 to be characterised by antiphase cyclicity relative to those with K_d above 1. However, day-night cycles in Mg/Ca are in phase with those in Sr/Ca and Ba/Ca and opposing to those in Na/Ca, even though Na and Mg have partition coefficients well below 1, while Sr is slightly above 1 and Ba well above 1 for inorganic precipitation at 25 °C (Gaetani and Cohen, 2006) and in corals (Giri et al., 2018; Ram and Erez, 2021). The pattern of Mg/Ca varying in phase with Sr/Ca and Ba/Ca indicates that a differential degree of Rayleigh fractionation at night is not the cause for the observed day-night cycles.

Additionally, we can demonstrate that the EPF is replenished by isotopically-labelled seawater during both day and night and is thus not a closed-of system at night. However, the different degree of tracer uptake, with 1.7 times higher $^{135}Ba/^{138}Ba$ peaks (i.e. closer to the ratio of the labelled seawater of 1.24) in day-spiked shells compared to those spiked at night, could indicate increased seawater intake and ion transport during the day (see Fig. 5).

The observed elemental banding patterns could also be cause by kinetic effects through trace element partitioning into aragonite, driven by changes in the aragonite precipitation rate. Increased precipitation rate causes increased incorporation of Na^{+} (Brazier et al., 2024) and Mg^{2+} (Mavromatis et al., 2022), while Sr incorporation broadly

https://doi.org/10.5194/egusphere-2025-3479
Preprint. Discussion started: 25 July 2025

decreases at higher growth rates (Brazier et al., 2023), although other studies have suggested a more complex response depending on temperature and solution chemistry (AlKhatib and Eisenhauer, 2017). As seen in a previous study (Arndt et al., 2023), Na/Ca in *Tridacna* seems to increase while Mg/Ca and Sr/Ca seem to decrease with increased growth rates. While uncertainties remain regarding kinetically-driven element incorporation, Na/Ca and Sr/Ca seem to follow the suggested trends, Mg/Ca is however opposing the trend expected from inorganic growth dynamics. For inorganic calcite precipitation it has also been suggested that Mg^{2+} incorporation into the structure reduces growth, while Sr incorporation increases growth (Knight et al., 2023). High [Mg] in the EPF during nighttime could thus be the cause not the effect of low growth rates.

Another explanation is that increased active Ca^{2+} pumping (possibly light enhanced) into the EPF during daytime reduces the relative concentration of other elements in the EPF (Sr, Ba, Mg, B) through dilution. This could explain how most elemental ratios (except Na/Ca) - independent of their fractionation factors and inorganic growth rate dynamics - decrease during the day when growth rates increase.

4.4.4 Why is Na different?

Na/Ca behaves differently than the other El/Ca as it decreases during the night. This may be because the Na^+-proton and Na^+-bicarbonate transporters are involved in controlling the carbonate chemistry of the EPF and maintaining charge balance in channelling Ca^{2+} (Ip and Chew, 2021). In *Tridacna* the pH of the EPF appears to be dependent, at least to a degree, on light, with pH being controlled through light dependent NH_4^+ channelling (Ip et al., 2006). In addition, the Na^+/H^+ Exchanger (βNHE) is active in pumping out H^+ and regulating pH within the seawater-facing epithelium of the mantle (Cao-Pham et al., 2019a), while light-dependent Na^+/H^+ exchangers are thought to be important in bringing inorganic carbon into the clam and to the photosymbionts (Hiong et al., 2017; Ip and Chew, 2021). Na^+ is also used for metal transport at the EPF-facing epithelium. Specifically, light enhanced activity of the NCX3 enzyme pumping Ca^{2+} into the EPF in exchange for Na^+ has been shown (Boo et al., 2019; Ip and Chew, 2021). NCX3 requires the support of Na^+/K^+-ATPase, which transports Na^+ back into the EPF and also shows light-enhanced activity (Boo et al., 2017). In addition, bicarbonate transport to the EPF may be an important carbon source for calcification, which may be achieved with the electrogenic $Na^+/HCO3^-$ co-transporter, further increasing Na^+ in the EPF during times of increased calcification (Ip and Chew, 2021). All of these processes may lead to a higher Na^+ concentration in the EPF during light exposure.

4.4.5 Potential mechanisms explaining the patterns

Overall, light enhanced Na^+ pumping coupled to Ca^{2+} and HCO_3^- transport might explain why Na/Ca is elevated during the day unlike other El/Ca (El = B, Mg, Sr, Ba). Together with a (possibly more minor role) of growth rate-related kinetic effects, we propose that light dependent Ca^{2+} and Na^+ transport and the dilution of other (trace) elements can explain the daily cycles in El/Ca seen here (Figs. 3,4) and previously reported (Arndt et al., 2023; Brosset et al., 2025; Hori et al., 2015; Sano et al., 2012; Warter et al., 2018; Warter and Müller, 2017; Yan, 2020). We assume that the same mechanism, namely the intensity of active Ca^{2+} and HCO_3^- channelling into the EPF, directs day and night changes in El composition, growth rate, shell structure and possibly organic content. An increase in calcification rate during the day, namely fivefold higher at day than at night for the clams cultured in this study (Tab. 2), could affect the crystal structure and might lead to a relatively lower content of template organics in the shell.

https://doi.org/10.5194/egusphere-2025-3479
Preprint. Discussion started: 25 July 2025

Light enhanced activation of important channelling enzymes could indicate that the formation of daily elemental cycles and increments is light dependent. It has, however, also been suggested that independent from environmental factors circadian rhythms are dictating diurnal changes (de Winter et al., 2023; Liu et al., 2024; Warter et al., 2018), with de Winter at al. (2023) observing that a shell grown under shades does not exhibit significantly different daily cycles. Energy consumption and light availability seem to be strongly coupled in *Tridacna* and thus it remains difficult to distinguish the impact of metabolic activity throughout the day from that of light availability.

4.5 Relative phasing of the daily increments and elemental cycles

An increase in trace element concentrations in bands grown at night has been based on the assumption that thinner bands likely represent the night growth, while thicker bands represent day growth in *Tridacna* (Brosset et al., 2025; Mills et al., 2024; Sano et al., 2012). While daytime shell growth was previously assumed to be about three times higher than at night (Brosset et al., 2025), our alkalinity measurements (conducted every 12 h) allow us to determine that the eight specimens utilised here grew on average five times faster regarding calcification in volume (Tab. 2), resulting in roughly 1.2 times higher accumulation of shell in the direction of growth during daytime versus nighttime (Figs. 3, 4).

We gain new insights about the detailed timing of the Mg/Ca and Sr/Ca increase and decrease over the course of a day by comparing the differential incorporation of the ^{135}Ba isotope tracer, supplied only during the day or during nighttime, to the Mg/Ca and Sr/Ca cycles within the shells. We can unequivocally confirm that Mg/Ca and Sr/Ca increase at nighttime in the narrower low growth bands, but the highest Mg/Ca values do not correspond to midnight, as previously suggested (e.g., Brosset et al., 2025). The clams that grew with the tracer introduced at nighttime (from 19:30 to 7:30) begin to incorporate the tracer into the shell approximately during the Mg/Ca and Sr/Ca minimum, with the tracer concentration decreasing within the shell shortly after the Mg/Ca and Sr/Ca maximum is reached. Similarly, the clams that grew in the presence of the tracer during the day (from 7:30 to 19:30) are characterised by a tracer onset in the shell approximately coincident with the Mg/Ca and Sr/Ca maximum. The tracer signal decreases shortly after the Mg/Ca and Sr/Ca minimum is reached. The isotopic tracer administered for 12 h each can only be incorporated as observed if the Mg/Ca and Sr/Ca maxima reflect the early morning hours or the end of the night, while the Mg/Ca and Sr/Ca minima are reached in the evening hours or towards the end of the day.

5 Conclusion

Our findings indicate that calcification rates in *Tridacna sp.* are nearly five times higher during the day compared to those at night. The EPF is replenished by surrounding seawater during both day and night, with the uptake and washout of elements starting quickly, likely within tens of minutes, but requiring approximately one day to fully replenish the EPFs composition. During daytime B/Ca, Mg/Ca, Sr/Ca and Ba/Ca decrease while Na/Ca increases and vice versa during nighttime. The night peak, often best seen in Mg/Ca, happens in the early morning hours not at midnight, while the day peak reflects the evening hours not the middle of the day. Daily El/Ca cycles might be affected by growth rate dynamics, while elemental compositions in the EPF could in turn affect growth rates. It is, however, likely that daily El/Ca cycles are primarily caused by changes in the intensity of active Ca^{2+} and HCO_3^- -channelling into the EPF, reducing most El/Ca through relatively higher Ca^{2+} availability during the day, except

https://doi.org/10.5194/egusphere-2025-3479
Preprint. Discussion started: 25 July 2025

Na^+ which is strongly involved in Ca^{2+}, HCO_3^- and H^+ channelling. The changes in active pumping into and from the EPF could in turn be dependent on light availability, circadian rhythms or simply be an expression of the energy available for channelling. We propose the active pumping of Ca^{2+} and HCO_3^- into the EPF might also cause diurnal changes in growth rate, organic content and shell structure. Overall, this study enhances the knowledge base for utilizing *Tridacna sp.* as a high-resolution paleoclimate archive, particularly for sub-daily time scale applications, by improving the spatial resolution of LA-ICPMS and deepening the understanding of diurnal growth patterns, variability in elemental composition, and rapid responses to environmental changes.

Competing interests

The authors declare that they have no conflict of interest.

Authors contributions

IA: Conceptualization, Data curation, Formal analysis, Funding acquisition, Investigation, Validation, Visualization, Writing (original draft preparation), Writing (review and editing); JE: Conceptualization, Funding acquisition, Investigation, Methodology, Project administration, Resources, Supervision, Validation, Writing (review and editing); DE: Conceptualization, Data curation, Supervision, Validation, Writing (review and editing); TE: Data curation, Investigation, Methodology, Supervision, Validation, Writing (review and editing); AL: Investigation, Validation, Writing (review and editing); WM: Conceptualization, Data curation, Funding acquisition, Methodology, Project administration, Resources, Supervision, Validation, Writing (review and editing)

Acknowledgements

We would like to acknowledge the Deutsche Forschungsgemeinschaft (DFG MU 3739/6-1) for their financial support of the corresponding author (IA) as well as the culturing experiments at the Hebrew University of Jerusalem (WM, JE). We also appreciate the support from the VeWA consortium (Past Warm Periods as Natural Analogues of our high-CO2 Climate Future), funded by the LOEWE programme of the Hessen Ministry of Higher Education, Research and the Arts, Germany (DE, WM). We gratefully acknowledge DFG Major Equipment Grant INST 161/1073-1 FUGG and Goethe University startup funding (both to WM), We thank Maria Bladt and Niels Prawitz for their valuable work in sample preparation. Additionally, we acknowledge Linda Marko and Alexander Schmidt for their technical support in the FIERCE laboratories. FIERCE is financially supported by the Wilhelm and Else Heraeus Foundation and by the Deutsche Forschungsgemeinschaft (DFG: INST 161/921-1 FUGG, INST 161/923-1 FUGG and INST 161/1073-1 FUGG), which is gratefully acknowledged.

References

Addadi, L., Joester, D., Nudelman, F., Weiner, S., 2006. Mollusk Shell Formation: A Source of New Concepts for Understanding Biomineralization Processes. Chemistry – A European Journal 12, 980–987. https://doi.org/10.1002/chem.200500980

Agbaje, O.B.A., Wirth, R., Morales, L.F.G., Shirai, K., Kosnik, M., Watanabe, T., Jacob, D.E., 2017. Architecture of crossed-lamellar bivalve shells: the southern giant clam (Tridacna derasa, Röding, 1798). R. Soc. open sci. 4. https://doi.org/10.1098/rsos.170622

https://doi.org/10.5194/egusphere-2025-3479
Preprint. Discussion started: 25 July 2025

Aharon, P., Chappell, J., 1986. Oxygen isotopes, sea level changes and the temperature history of a coral reef environment in New Guinea over the last 105 years. Palaeogeography, Palaeoclimatology, Palaeoecology 56, 337–379. https://doi.org/10.1016/0031-0182(86)90101-X

AlKhatib, M., Eisenhauer, A., 2017. Calcium and strontium isotope fractionation during precipitation from aqueous solutions as a function of temperature and reaction rate; II. Aragonite. Geochimica et Cosmochimica Acta 209, 320–342. https://doi.org/10.1016/j.gca.2017.04.012

Arndt, I., Bernecker, M., Erhardt, T., Evans, D., Fiebig, J., Fursman, M., Kniest, J., Renema, W., Schlidt, V., Staudigel, P., Voigt, S., Müller, W., 2025. 20,000 days in the life of a giant clam reveal late Miocene tropical climate variability. Palaeogeography, Palaeoclimatology, Palaeoecology 112711. https://doi.org/10.1016/j.palaeo.2024.112711

Arndt, I., Coenen, D., 2023. Daydacna. https://doi.org/10.5281/ZENODO.8334594

Arndt, I., Coenen, D., Evans, D., Renema, W., Müller, W., 2023. Quantifying Sub-Seasonal Growth Rate Changes in Fossil Giant Clams Using Wavelet Transformation of Daily Mg/Ca Cycles. Geochemistry, Geophysics, Geosystems 24, e2023GC010992. https://doi.org/10.1029/2023GC010992

Ayling, B.F., Chappell, J., Gagan, M.K., McCulloch, M.T., 2015. ENSO variability during MIS 11 (424–374 ka) from *Tridacna gigas* at Huon Peninsula, Papua New Guinea. EPSL 431, 236–246. https://doi.org/10.1016/j.epsl.2015.09.037

Bonham, K., 1965. Growth Rate of Giant Clam Tridacna gigas at Bikini Atoll as Revealed by Radioautography. Science 149, 300–302. https://doi.org/10.1126/science.149.3681.300

Boo, M.V., Chew, S.F., Ip, Y.K., 2021. Basolateral Na+/Ca2+ exchanger 1 and Na+/K+-ATPase, which display light-enhanced gene and protein expression levels, could be involved in the absorption of exogenous Ca2+ through the ctenidium of the giant clam, *Tridacna squamosa*. Comparative Biochemistry and Physiology Part A: Molecular & Integrative Physiology 259, 110997. https://doi.org/10.1016/j.cbpa.2021.110997

Boo, M.V., Hiong, K.C., Choo, C.Y.L., Cao-Pham, A.H., Wong, W.P., Chew, S.F., Ip, Y.K., 2017. The inner mantle of the giant clam, Tridacna squamosa, expresses a basolateral Na+/K+-ATPase α-subunit, which displays light-dependent gene and protein expression along the shell-facing epithelium. PLOS ONE 12, e0186865. https://doi.org/10.1371/journal.pone.0186865

Boo, M.V., Hiong, K.C., Wong, W.P., Chew, S.F., Ip, Y.K., 2019. Shell formation in the giant clam, Tridacna squamosa, may involve an apical Na+/Ca2+ exchanger 3 homolog in the shell-facing epithelium of the whitish inner mantle, which displays light-enhanced gene and protein expression. Coral Reefs 38, 1173–1186. https://doi.org/10.1007/s00338-019-01848-y

Boo, M.V., Pang, C.Z., Chew, S.F., Ip, Y.K., 2022. Molecular characterization, immunofluorescent localization, and expression levels of two bicarbonate anion transporters in the whitish mantle of the giant clam, *Tridacna squamosa*, and the implications for light-enhanced shell formation. Comparative Biochemistry and Physiology Part A: Molecular & Integrative Physiology 268, 111200. https://doi.org/10.1016/j.cbpa.2022.111200

Brazier, J.-M., Blanchard, M., Méheut, M., Schmitt, A.-D., Schott, J., Mavromatis, V., 2023. Experimental and theoretical investigations of stable Sr isotope fractionation during its incorporation in aragonite. Geochimica et Cosmochimica Acta 358, 134–147. https://doi.org/10.1016/j.gca.2023.08.013

Brazier, J.-M., Harrison, A.L., Rollion-Bard, C., Mavromatis, V., 2024. Controls of temperature and mineral growth rate on lithium and sodium incorporation in abiotic aragonite. Chemical Geology 654, 122057. https://doi.org/10.1016/j.chemgeo.2024.122057

Brosset, C., Liu, C., Yang, H., Yan, H., Schöne, B.R., 2025. Integrating high-resolution Sr/Ca and ultrastructural analyses of the *Tridacna squamosa* shell to reconstruct sub-daily seawater temperature variation. Palaeogeography, Palaeoclimatology, Palaeoecology 659, 112663. https://doi.org/10.1016/j.palaeo.2024.112663

Cao-Pham, A.H., Hiong, K.C., Boo, M.V., Choo, C.Y.L., Pang, C.Z., Wong, W.P., Neo, M.L., Chew, S.F., Ip, Y.K., 2019. Molecular characterization, cellular localization, and light-enhanced expression of Beta-Na+/H+ Exchanger-like in the whitish inner mantle of the giant clam, Tridacna squamosa, denote its role in light-enhanced shell formation. Gene 695, 101–112. https://doi.org/10.1016/j.gene.2019.02.009

Caswell, T.A., Droettboom, M., Lee, A., Andrade, E.S. de, Hoffmann, T., Klymak, J., Hunter, J., Firing, E., Stansby, D., Varoquaux, N., Nielsen, J.H., Root, B., May, R., Elson, P., Seppänen, J.K., Dale, D., Lee, J.-J., McDougall, D., Straw, A., Hobson, P., hannah, Gohlke, C., Vincent, A.F., Yu, T.S., Ma, E., Silvester, S., Moad, C., Kniazev, N., Ernest, E., Ivanov, P., 2022. matplotlib/matplotlib: REL: v3.5.2. https://doi.org/10.5281/zenodo.6513224

Chan, J.W.J., Boo, M.V., Wong, W.P., Chew, S.F., Ip, Y.K., 2021. Illumination enhances the protein abundance of sarcoplasmic reticulum Ca2+-ATPases-like transporter in the ctenidium and whitish inner mantle of the giant clam, *Tridacna squamosa*, to augment exogenous Ca2+ uptake and shell formation, respectively. Comparative Biochemistry and Physiology Part A: Molecular & Integrative Physiology 251, 110811. https://doi.org/10.1016/j.cbpa.2020.110811

https://doi.org/10.5194/egusphere-2025-3479
Preprint. Discussion started: 25 July 2025

Chew, S.F., Koh, C.Z.Y., Hiong, K.C., Choo, C.Y.L., Wong, W.P., Neo, M.L., Ip, Y.K., 2019. Light-enhanced expression of Carbonic Anhydrase 4-like supports shell formation in the fluted giant clam Tridacna squamosa. Gene 683, 101–112. https://doi.org/10.1016/j.gene.2018.10.023

de Winter, N.J., Killam, D., Fröhlich, L., de Nooijer, L., Boer, W., Schöne, B.R., Thébault, J., Reichart, G.-J., 2023. Ultradian rhythms in shell composition of photosymbiotic and non-photosymbiotic mollusks. Biogeosciences 20, 3027–3052. https://doi.org/10.5194/bg-20-3027-2023

Duprey, N., Lazareth, C.E., Dupouy, C., Butscher, J., Farman, R., Maes, C., Cabioch, G., 2015. Calibration of seawater temperature and $\delta^{18}O_{seawater}$ signals in *Tridacna maxima's* $\delta^{18}O_{shell}$ record based on in situ data. Coral Reefs 34, 437–450. https://doi.org/10.1007/s00338-014-1245-z

Elliot, M., Welsh, K., Chilcott, C., McCulloch, M., Chappell, J., Ayling, B., 2009. Profiles of trace elements and stable isotopes derived from giant long-lived *Tridacna gigas* bivalves: Potential applications in paleoclimate studies. Palaeogeography, Palaeoclimatology, Palaeoecology 280, 132–142. https://doi.org/10.1016/j.palaeo.2009.06.007

Evans, D., Brierley, C., Raymo, M.E., Erez, J., Müller, W., 2016. Planktic foraminifera shell chemistry response to seawater chemistry: Pliocene–Pleistocene seawater Mg/Ca, temperature and sea level change. Earth and Planetary Science Letters 438, 139–148. https://doi.org/10.1016/j.epsl.2016.01.013

Evans, D., Erez, J., Oron, S., Müller, W., 2015. Mg/Ca-temperature and seawater-test chemistry relationships in the shallow-dwelling large benthic foraminifera Operculina ammonoides. Geochimica et Cosmochimica Acta 148, 325–342. https://doi.org/10.1016/j.gca.2014.09.039

Evans, D., Gray, W.R., Rae, J.W.B., Greenop, R., Webb, P.B., Penkman, K., Kröger, R., Allison, N., 2020. Trace and major element incorporation into amorphous calcium carbonate (ACC) precipitated from seawater. Geochimica et Cosmochimica Acta 290, 293–311. https://doi.org/10.1016/j.gca.2020.08.034

Evans, D., Müller, W., 2018. Automated Extraction of a Five-Year LA-ICP-MS Trace Element Data Set of Ten Common Glass and Carbonate Reference Materials: Long-Term Data Quality, Optimisation and Laser Cell Homogeneity. Geostandards and Geoanalytical Research 42, 159–188. https://doi.org/10.1111/ggr.12204

Fehrenbacher, J.S., Russell, A.D., Davis, C.V., Gagnon, A.C., Spero, H.J., Cliff, J.B., Zhu, Z., Martin, P., 2017. Link between light-triggered Mg-banding and chamber formation in the planktic foraminifera Neogloboquadrina dutertrei. Nat Commun 8, 15441. https://doi.org/10.1038/ncomms15441

Fousiya, A.A., Malik, J.N., Paul, D., Chakraborty, S., Achyuthan, H., 2024. Microstructure and growth rate variability in a giant clam (Tridacna maxima) from the Lakshadweep Archipelago, India: implications for their use as biological monitors to trace extreme weather events. Coral Reefs. https://doi.org/10.1007/s00338-023-02455-8

Fursman, M., Warter, V., Janse, M., Renema, W., Spötl, C., Arndt, I., Evans, D., Müller, W., 2025. Ten years of *Tridacna* sclerochemistry at up to daily resolution from a controlled aquarium environment – Records of habitat change, induced seasonality and growth variability. Palaeogeography, Palaeoclimatology, Palaeoecology 675, 113022. https://doi.org/10.1016/j.palaeo.2025.113022

Gaetani, G.A., Cohen, A.L., 2006. Element partitioning during precipitation of aragonite from seawater: A framework for understanding paleoproxies. Geochimica et Cosmochimica Acta 70, 4617–4634. https://doi.org/10.1016/j.gca.2006.07.008

Gannon, M.E., Pérez-Huerta, A., Aharon, P., Street, S.C., 2017. A biomineralization study of the Indo-Pacific giant clam *Tridacna gigas*. Coral Reefs 36, 503–517. https://doi.org/10.1007/s00338-016-1538-5

Giri, S.J., Swart, P.K., Devlin, Q.B., 2018. The effect of changing seawater Ca and Mg concentrations upon the distribution coefficients of Mg and Sr in the skeletons of the scleractinian coral *Pocillopora damicornis*. Geochimica et Cosmochimica Acta 222, 535–549. https://doi.org/10.1016/j.gca.2017.11.011

Griffiths, N., Müller, W., Johnson, K.G., Aguilera, O.A., 2013. Evaluation of the effect of diagenetic cements on element/Ca ratios in aragonitic Early Miocene (~16Ma) Caribbean corals: Implications for 'deep-time' palaeo-environmental reconstructions. Palaeogeography, Palaeoclimatology, Palaeoecology 369, 185–200. https://doi.org/10.1016/j.palaeo.2012.10.018

Harris, C.R., Millman, K.J., van der Walt, S.J., Gommers, R., Virtanen, P., Cournapeau, D., Wieser, E., Taylor, J., Berg, S., Smith, N.J., Kern, R., Picus, M., Hoyer, S., van Kerkwijk, M.H., Brett, M., Haldane, A., del Río, J.F., Wiebe, M., Peterson, P., Gérard-Marchant, P., Sheppard, K., Reddy, T., Weckesser, W., Abbasi, H., Gohlke, C., Oliphant, T.E., 2020. Array programming with NumPy. Nature 585, 357–362. https://doi.org/10.1038/s41586-020-2649-2

Harzhauser, M., Mandic, O., Piller, W.E., Reuter, M., Kroh, A., 2008. Tracing Back the Origin of the Indo-Pacific Mollusc Fauna: Basal Tridacninae from the Oligocene and Miocene of the Sultanate of Oman. Palaeontology 51, 199–213. https://doi.org/10.1111/j.1475-4983.2007.00742.x

Hauzer, H., Evans, D., Müller, W., Rosenthal, Y., Erez, J., 2021. Salinity Effect on Trace Element Incorporation in Cultured Shells of the Large Benthic Foraminifer Operculina ammonoides. Paleoceanography and Paleoclimatology 36, e2021PA004218. https://doi.org/10.1029/2021PA004218

https://doi.org/10.5194/egusphere-2025-3479
Preprint. Discussion started: 25 July 2025

Hauzer, H., Evans, D., Müller, W., Rosenthal, Y., Erez, J., 2018. Calibration of Na partitioning in the calcitic foraminifer Operculina ammonoides under variable Ca concentration: Toward reconstructing past seawater composition. Earth and Planetary Science Letters 497, 80–91. https://doi.org/10.1016/j.epsl.2018.06.004

Hiong, K.C., Cao-Pham, A.H., Choo, C.Y.L., Boo, M.V., Wong, W.P., Chew, S.F., Ip, Y.K., 2017. Light-dependent expression of a Na+/H+ exchanger 3-like transporter in the ctenidium of the giant clam, Tridacna squamosa, can be related to increased H+ excretion during light-enhanced calcification. Physiological Reports 5, e13209. https://doi.org/10.14814/phy2.13209

Hori, M., Sano, Y., Ishida, A., Takahata, N., Shirai, K., Watanabe, T., 2015. Middle Holocene daily light cycle reconstructed from the strontium/calcium ratios of a fossil giant clam shell. Scientific Reports 5, 8734. https://doi.org/10.1038/srep08734

Ip, Y.K., Chew, S.F., 2021. Light-Dependent Phenomena and Related Molecular Mechanisms in Giant Clam-Dinoflagellate Associations: A Review. Front. Mar. Sci. 8. https://doi.org/10.3389/fmars.2021.627722

Ip, Y.K., Ching, B., Hiong, K.C., Choo, C.Y.L., Boo, M.V., Wong, W.P., Chew, S.F., 2015. Light induces changes in activities of Na+/K+-ATPase, H+/K+-ATPase and glutamine synthetase in tissues involved directly or indirectly in light-enhanced calcification in the giant clam, Tridacna squamosa. Front. Physiol. 6. https://doi.org/10.3389/fphys.2015.00068

Ip, Y.K., Hiong, K.C., Goh, E.J.K., Boo, M.V., Choo, C.Y.L., Ching, B., Wong, W.P., Chew, S.F., 2017. The Whitish Inner Mantle of the Giant Clam, Tridacna squamosa, Expresses an Apical Plasma Membrane Ca2+-ATPase (PMCA) Which Displays Light-Dependent Gene and Protein Expressions. Front. Physiol. 8. https://doi.org/10.3389/fphys.2017.00781

Ip, Y.K., Loong, A.M., Hiong, K.C., Wong, W.P., Chew, S.F., Reddy, K., Sivaloganathan, B., Ballantyne, J.S., 2006. Light Induces an Increase in the pH of and a Decrease in the Ammonia Concentration in the Extrapallial Fluid of the Giant Clam Tridacna squamosa. Physiological and Biochemical Zoology 79, 656–664. https://doi.org/10.1086/501061

Jantzen, C., Wild, C., El-Zibdah, M., Roa-Quiaoit, H.A., Haacke, C., Richter, C., 2008. Photosynthetic performance of giant clams, *Tridacna maxima* and *T. squamosa*, Red Sea. Mar Biol 155, 211–221. https://doi.org/10.1007/s00227-008-1019-7

Jochum, K.P., Scholz, D., Stoll, B., Weis, U., Wilson, S.A., Yang, Q., Schwalb, A., Börner, N., Jacob, D.E., Andreae, M.O., 2012. Accurate trace element analysis of speleothems and biogenic calcium carbonates by LA-ICP-MS. Chemical Geology 318–319, 31–44. https://doi.org/10.1016/j.chemgeo.2012.05.009

Jochum, K.P., Stoll, B., Herwig, K., Willbold, M., Hofmann, A.W., Amini, M., Aarburg, S., Abouchami, W., Hellebrand, E., Mocek, B., Raczek, I., Stracke, A., Alard, O., Bouman, C., Becker, S., Dücking, M., Brätz, H., Klemd, R., de Bruin, D., Canil, D., Cornell, D., de Hoog, C.-J., Dalpé, C., Danyushevsky, L., Eisenhauer, A., Gao, Y., Snow, J.E., Groschopf, N., Günther, D., Latkoczy, C., Guillong, M., Hauri, E.H., Höfer, H.E., Lahaye, Y., Horz, K., Jacob, D.E., Kasemann, S.A., Kent, A.J.R., Ludwig, T., Zack, T., Mason, P.R.D., Meixner, A., Rosner, M., Misawa, K., Nash, B.P., Pfänder, J., Premo, W.R., Sun, W.D., Tiepolo, M., Vannucci, R., Vennemann, T., Wayne, D., Woodhead, J.D., 2006. MPI-DING reference glasses for in situ microanalysis: New reference values for element concentrations and isotope ratios. Geochemistry, Geophysics, Geosystems 7. https://doi.org/10.1029/2005GC001060

Jochum, K.P., Weis, U., Stoll, B., Kuzmin, D., Yang, Q., Raczek, I., Jacob, D.E., Stracke, A., Birbaum, K., Frick, D.A., Günther, D., Enzweiler, J., 2011. Determination of Reference Values for NIST SRM 610–617 Glasses Following ISO Guidelines. Geostandards and Geoanalytical Research 35, 397–429. https://doi.org/10.1111/j.1751-908X.2011.00120.x

Killam, D., Al-Najjar, T., Clapham, M., 2021. Giant clam growth in the Gulf of Aqaba is accelerated compared to fossil populations. Proceedings of the Royal Society B: Biological Sciences 288, 20210991. https://doi.org/10.1098/rspb.2021.0991

Killam, D., Thompson, D., Morgan, K., Russell, M., 2023. Giant clams as open-source, scalable reef environmental biomonitors. PLOS ONE 18, e0278752. https://doi.org/10.1371/journal.pone.0278752

Klumpp, D., Griffiths, C., 1994. Contributions of phototrophic and heterotrophic nutrition to the metabolic and growth requirements of four species of giant clam (Tridacnidae). Mar. Ecol. Prog. Ser. 115, 103–115. https://doi.org/10.3354/meps115103

Klumpp, D.W., Bayne, B.L., Hawkins, A.J.S., 1992. Nutrition of the giant clam Tridacna gigas (L.) I. Contribution of filter feeding and photosynthates to respiration and growth. Journal of Experimental Marine Biology and Ecology 155, 105–122. https://doi.org/10.1016/0022-0981(92)90030-E

Knight, A.W., Harvey, J.A., Shohel, M., Lu, P., Cummings, D., Ilgen, A.G., 2023. The combined effects of Mg2+ and Sr2+ incorporation during CaCO3 precipitation and crystal growth. Geochimica et Cosmochimica Acta 345, 16–33. https://doi.org/10.1016/j.gca.2023.01.021

Kobayashi, I., Samata, T., 2006. Bivalve shell structure and organic matrix. Materials Science and Engineering: C, Second Asian Symposium on Biomineralization (ASB-2) 26, 692–698. https://doi.org/10.1016/j.msec.2005.09.101

https://doi.org/10.5194/egusphere-2025-3479
Preprint. Discussion started: 25 July 2025

Kunzmann, A., 2008. Physiological performance of giant clams (Tridacna spec.) in a recirculation system, in: ICRS Conference Proceedings. Presented at the 11th International Coral Reef Symposium, Ft. Lauderdale, Florida, pp. 316–320.

Levi, A., Müller, W., Erez, J., 2019. Intrashell Variability of Trace Elements in Benthic Foraminifera Grown Under High CO2 Levels. Front. Earth Sci. 7, 247. https://doi.org/10.3389/feart.2019.00247

Liu, C., Yan, H., Zhao, L., Zhao, N., Luo, F., Wen, H., Yang, H., Yang, W., Hao, J., Liang, C., Tanaka, K., Murakami-Sugihara, N., Shirai, K., Takahata, N., Dodson, J., Schöne, B.R., 2024. Potential environment effect on ultrahigh resolution Sr/Ca of giant clam shells from South China Sea. Coral Reefs. https://doi.org/10.1007/s00338-024-02555-z

Liu, C., Zhao, L., Zhao, N., Yang, W., Hao, J., Qu, X., Liu, S., Dodson, J., Yan, H., 2022. Novel methods of resolving daily growth patterns in giant clam (Tridacna spp.) shells. Ecological Indicators 134, 108480. https://doi.org/10.1016/j.ecolind.2021.108480

Longerich, H.P., Jackson, S.E., Günther, D., 1996. Inter-laboratory note. Laser ablation inductively coupled plasma mass spectrometric transient signal data acquisition and analyte concentration calculation. J. Anal. At. Spectrom. 11, 899–904. https://doi.org/10.1039/JA9961100899

Ma, X., Yan, H., Fei, H., Liu, C., Shi, G., Huang, E., Wang, Y., Qu, X., Lian, E., Dang, H., 2020. A high-resolution $\delta^{18}O$ record of modern *Tridacna gigas* bivalve and its paleoenvironmental implications. Palaeogeography, Palaeoclimatology, Palaeoecology 554. https://doi.org/10.1016/j.palaeo.2020.109800

Mavromatis, V., Brazier, J.-M., Goetschl, K.E., 2022. Controls of temperature and mineral growth rate on Mg incorporation in aragonite. Geochimica et Cosmochimica Acta 317, 53–64. https://doi.org/10.1016/j.gca.2021.10.015

Mills, K., John, E.H., Muir, D.D., Santodomingo, N., Johnson, K.G., Hussein, M.A.S., Sosdian, S., 2023. Growth responses of mixotrophic giant clams on nearshore turbid coral reefs. Coral Reefs 42, 592–608. https://doi.org/10.1007/s00338-023-02366-8

Mills, K., Muir, D.D., Oldroyd, A., John, E.H., Santodomingo, N., Johnson, K.G., Hussein, M.A.S., Sosdian, S., 2024. Microstructure and crystallographic texture data in modern giant clam shells (*Tridacna squamosa* and *Hippopus hippopus*). Data in Brief 52, 109947. https://doi.org/10.1016/j.dib.2023.109947

Müller, W., Shelley, M., Miller, P., Broude, S., 2009. Initial performance metrics of a new custom-designed ArF excimer LA-ICPMS system coupled to a two-volume laser-ablation cell. Journal of Analytical Atomic Spectrometry 24, 209–214. https://doi.org/10.1039/B805995K

Norris, C.A., Danyushevsky, L., Olin, P., West, N.R., 2021. Elimination of aliasing in LA-ICP-MS by alignment of laser and mass spectrometer. J. Anal. At. Spectrom. 36, 733–739. https://doi.org/10.1039/D0JA00488J

Paton, C., Hellstrom, J., Paul, B., Woodhead, J., Hergt, J., 2011. Iolite: Freeware for the visualisation and processing of mass spectrometric data. J. Anal. At. Spectrom. 26, 2508–2518. https://doi.org/10.1039/C1JA10172B

Pätzold, J., Heinrichs, J.P., Wolschendorf, K., Wefer, G., 1991. Correlation of stable oxygen isotope temperature record with light attenuation profiles in reef-dwelling *Tridacna* shells. Coral Reefs 10, 65–69. https://doi.org/10.1007/BF00571825

Ram, S., Erez, J., 2021. The Distribution Coefficients of Major and Minor Elements in Coral Skeletons Under Variable Calcium Seawater Concentrations. Frontiers in Earth Science 9, 336. https://doi.org/10.3389/feart.2021.657176

Reback, J., jbrockmendel, McKinney, W., Bossche, J.V. den, Roeschke, M., Augspurger, T., Hawkins, S., Cloud, P., gfyoung, Sinhrks, Hoefler, P., Klein, A., Petersen, T., Tratner, J., She, C., Ayd, W., Naveh, S., Darbyshire, J.H.M., Shadrach, R., Garcia, M., Schendel, J., Hayden, A., Saxton, D., Gorelli, M.E., Li, F., Wörtwein, T., Zeitlin, M., Jancauskas, V., McMaster, A., Li, T., 2022. pandas-dev/pandas: Pandas 1.4.3. https://doi.org/10.5281/zenodo.6702671

Rosewater, J., 1965. The Family Tridacnidae in the Indo-Pacific. Indo-Pacific Mollusca 1, 153.

Rossbach, S., Saderne, V., Anton, A., Duarte, C.M., 2019. Light-dependent calcification in Red Sea giant clam *Tridacna maxima*. Biogeosciences 16, 2635–2650. https://doi.org/10.5194/bg-16-2635-2019

Sano, Y., Kobayashi, S., Shirai, K., Takahata, N., Matsumoto, K., Watanabe, T., Sowa, K., Iwai, K., 2012. Past daily light cycle recorded in the strontium/calcium ratios of giant clam shells. Nature Communications 3, 761. https://doi.org/10.1038/ncomms1763

Savitzky, Abraham., Golay, M.J.E., 1964. Smoothing and Differentiation of Data by Simplified Least Squares Procedures. Anal. Chem. 36, 1627–1639. https://doi.org/10.1021/ac60214a047

Schleinkofer, N., Raddatz, J., Evans, D., Gerdes, A., Flögel, S., Voigt, S., Büscher, J.V., Wisshak, M., 2021. Compositional variability of Mg/Ca, Sr/Ca, and Na/Ca in the deep-sea bivalve Acesta excavata (Fabricius, 1779). PLOS ONE 16, e0245605. https://doi.org/10.1371/journal.pone.0245605

Schöne, B.R., Zhang, Z., Jacob, D., Gillikin, D.P., TÜTKEN, T., GARBE-SCHÖNBERG, D., Mcconnaughey, T., Soldati, A., 2010. Effect of organic matrices on the determination of the trace element chemistry (Mg, Sr, Mg/Ca, Sr/Ca) of aragonitic bivalve shells (Arctica islandica) Comparison of ICP-OES and LA-ICP-MS data. Geochem. J. 44, 23–37. https://doi.org/10.2343/geochemj.1.0045

https://doi.org/10.5194/egusphere-2025-3479
Preprint. Discussion started: 25 July 2025

Schwartzmann, C., Durrieu, G., Sow, M., Ciret, P., Lazareth, C.E., Massabuau, J.-C., 2011. In situ giant clam growth rate behavior in relation to temperature: A one-year coupled study of high-frequency noninvasive valvometry and sclerochronology. Limnology and Oceanography 56, 1940–1951. https://doi.org/10.4319/lo.2011.56.5.1940

Shirai, K., Schöne, B.R., Miyaji, T., Radarmacher, P., Krause, R.A., Tanabe, K., 2014. Assessment of the mechanism of elemental incorporation into bivalve shells (*Arctica islandica*) based on elemental distribution at the microstructural scale. Geochimica et Cosmochimica Acta 126, 307–320. https://doi.org/10.1016/j.gca.2013.10.050

Silverman, J., Lazar, B., Erez, J., 2007. Community metabolism of a coral reef exposed to naturally varying dissolved inorganic nutrient loads. Biogeochemistry 84, 67–82. https://doi.org/10.1007/s10533-007-9075-5

Stephenson, A.E., DeYoreo, J.J., Wu, L., Wu, K.J., Hoyer, J., Dove, P.M., 2008. Peptides Enhance Magnesium Signature in Calcite: Insights into Origins of Vital Effects. Science 322, 724–727. https://doi.org/10.1126/science.1159417

Van Wynsberge, S., Andréfouët, S., Gaertner-Mazouni, N., Wabnitz, C.C.C., Menoud, M., Le Moullac, G., Levy, P., Gilbert, A., Remoissenet, G., 2017. Growth, Survival and Reproduction of the Giant Clam Tridacna maxima (Röding 1798, Bivalvia) in Two Contrasting Lagoons in French Polynesia. PLoS One 12, e0170565. https://doi.org/10.1371/journal.pone.0170565

Veeh, H.H., Chappell, J., 1970. Astronomical Theory of Climatic Change: Support from New Guinea. Science 167, 862–865. https://doi.org/10.1126/science.167.3919.862

Wang, D., Wallace, A.F., De Yoreo, J.J., Dove, P.M., 2009. Carboxylated molecules regulate magnesium content of amorphous calcium carbonates during calcification. Proceedings of the National Academy of Sciences 106, 21511–21516. https://doi.org/10.1073/pnas.0906741106

Warter, V., Erez, J., Müller, W., 2018. Environmental and physiological controls on daily trace element incorporation in *Tridacna crocea* from combined laboratory culturing and ultra-high resolution LA-ICP-MS analysis. Palaeogeography, Palaeoclimatology, Palaeoecology 496, 32–47. https://doi.org/10.1016/j.palaeo.2017.12.038

Warter, V., Müller, W., 2017. Daily growth and tidal rhythms in Miocene and modern giant clams revealed via ultra-high resolution LA-ICPMS analysis — A novel methodological approach towards improved sclerochemistry. Palaeogeography, Palaeoclimatology, Palaeoecology 465, 362–375. https://doi.org/10.1016/j.palaeo.2016.03.019

Warter, V., Müller, W., Wesselingh, F.P., Todd, J.A., Renema, W., 2015. Late Miocene seasonal to subdecadal climate variability in the Indo-West Pacific (East Kalimantan, Indonesia) preserved in giant clams. PALAIOS 30, 66–82. https://doi.org/10.2110/palo.2013.061

Watanabe, T., Oba, T., 1999. Daily reconstruction of water temperature from oxygen isotopic ratios of a modern Tridacna shell using a freezing microtome sampling technique. Journal of Geophysical Research: Oceans 104, 20667–20674. https://doi.org/10.1029/1999JC900097

Watanabe, T., Suzuki, A., Kawahata, H., Kan, H., Ogawa, S., 2004. A 60-year isotopic record from a mid-Holocene fossil giant clam (Tridacna gigas) in the Ryukyu Islands: physiological and paleoclimatic implications. Palaeogeography, Palaeoclimatology, Palaeoecology 212, 343–354. https://doi.org/10.1016/j.palaeo.2004.07.001

Weiss, I.M., Tuross, N., Addadi, L., Weiner, S., 2002. Mollusc larval shell formation: amorphous calcium carbonate is a precursor phase for aragonite. J Exp Zool 293, 478–491. https://doi.org/10.1002/jez.90004

Welsh, K., Elliot, M., Tudhope, A., Ayling, B., Chappell, J., 2011. Giant bivalves (Tridacna gigas) as recorders of ENSO variability. EPSL 307, 266–270. https://doi.org/10.1016/j.epsl.2011.05.032

Yan, H., 2020. Daily growth bands of giant clam shell: A potential paleoweather recorder. Solid Earth Sciences 5, 249–253. https://doi.org/10.1016/j.sesci.2020.10.001

Yan, H., Liu, C., An, Z., Yang, W., Yang, Yuanjian, Huang, P., Qiu, S., Zhou, P., Zhao, N., Fei, H., Ma, X., Shi, G., Dodson, J., Hao, J., Yu, K., Wei, G., Yang, Yanan, Jin, Z., Zhou, W., 2020. Extreme weather events recorded by daily to hourly resolution biogeochemical proxies of marine giant clam shells. Proc Natl Acad Sci USA 117, 7038–7043. https://doi.org/10.1073/pnas.1916784117

Yan, H., Zhao, N., Zhou, P., Liu, C., Fei, H., Li, M., Liu, F., Yang, Y., Yang, W., Dodson, J., 2021. The first detection of the Madden-Julian Oscillation signal in daily to hourly resolution proxy records derived from a natural archive of Giant Clam Shell (Tridacna spp.). Earth and Planetary Science Letters 555, 116703. https://doi.org/10.1016/j.epsl.2020.116703

Zhao, N., Yan, H., Luo, F., Yang, Y., Liu, S., Zhou, P., Liu, C., Dodson, J., 2023. Daily growth rate variation in *Tridacna* shells as a record of tropical cyclones in the South China Sea: Palaeoecological implications. Palaeogeography, Palaeoclimatology, Palaeoecology 615, 111444. https://doi.org/10.1016/j.palaeo.2023.111444

Zhao, N., Yan, H., Yang, Y., Liu, C., Ma, X., Wang, G., Zhou, P., Wen, H., Qu, X., Dodson, J., 2021. A 23.7-year long daily growth rate record of a modern giant clam shell from South China Sea and its potential in high-

https://doi.org/10.5194/egusphere-2025-3479
Preprint. Discussion started: 25 July 2025

resolution paleoclimate reconstruction. Palaeogeography, Palaeoclimatology, Palaeoecology 583, 110682. https://doi.org/10.1016/j.palaeo.2021.110682